NANO LETTERS

Letter

pubs.acs.org/NanoLett

Quantized Conductance in an InSb Nanowire

Ilse van Weperen,[†] Sébastien R. Plissard,[‡] Erik P. A. M. Bakkers,[†,‡] Sergey M. Frolov,[†,§] and Leo P. Kouwenhoven*[,†]

[†]Kavli Institute of Nanoscience, Delft University of Technology, 2600 GA Delft, The Netherlands

[‡]Department of Applied Physics, Eindhoven University of Technology, 5600 MB Eindhoven, The Netherlands

Supporting Information

ABSTRACT: Ballistic one-dimensional transport in semiconductor nanowires plays a central role in creating topological and helical states. The hallmark of such one-dimensional transport is conductance quantization. Here we show conductance quantization in InSb nanowires at nonzero magnetic fields. Conductance plateaus are studied as a function of source-drain bias and magnetic field, enabling extraction of the Landé g factor and the subband spacing.

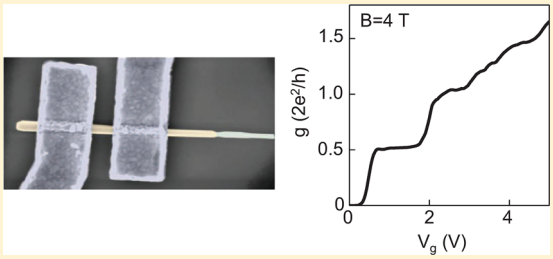

KEYWORDS: *Conductance quantization, ballistic transport, quantum point contact, subband, nanowire, InSb*

Semiconductor nanowires are the starting point of recently proposed topological systems.[1−3] A topological superconducting region arises in a one-dimensional (1D) semiconductor wire in the presence of a strong spin−orbit coupling when it is brought in contact with a superconducting material. On the boundary of the topological and nontopological wire regions Majorana fermions (MFs) are expected.[4] The MFs in a nanowire, quasi-particles that are an equal superposition of an electron and a hole, are candidate building blocks for fault-tolerant quantum computation.[4,5] Moreover, 1D semiconductor wires with strong spin−orbit coupling have also been identified as a suitable platform for creation of a helical state.[6−8] In such a state spin and momentum of an electron are perfectly correlated, thereby creating spin polarization and allowing spin filtering, key themes in the field of spintronics.[9−11]

InSb nanowires, alongside InAs and Si/Ge core−shell nanowires, are promising for study of topological and helical states, as they have a strong spin−orbit interaction,[12] and superconductivity can be induced in the nanowires.[13] Indeed signatures of MFs have been reported in hybrid semiconductor−superconductor InSb nanowire devices.[14] While in InSb nanowires the basic properties of spin−orbit interaction and induced superconductivity have each been separately investigated, the degree of fulfillment of the third requirement for creation of MFs, the 1D semiconductor wire, is not as well understood. In a 1D wire transport takes place in subbands, of which the occupation is controlled by an external gate voltage. While first schemes for detection of MFs required occupation of only a single subband near the superconducting contacts where the MFs form,[1,2] later proposals extended this condition to the multisubband regime.[15−17] Information about the energy spectrum of InSb nanowires needed to answer questions of subband occupation is however lacking. Moreover, MFs are affected by disorder in the wire,[17−19] of which the extent is unknown. Such disorder creates diffusive transport, instead of the ballistic transport implied in the 1D requirement. Subband occupation and disorder are also key issues in creation of helical states in InSb nanowires.

The formation of subbands in (ballistic) 1D wires is shown in transport measurements by quantization of conductance, where each spin-degenerate subband contributes a conductance of $g_Q = 2e^2/h$.[20,21] In semiconductor nanowires conductance quantization is hard to achieve, as it requires strong suppression of disorder between source and drain contact, a distance of typically several hundred nanometers to a few micrometers. Disorder, both due to structural imperfections and surface states,[22,23] leads to scattering of electrons, which due to the radial confinement of nanowires often results in reflection of electrons back to the reservoir from which they originated, that is, backscattering (Figure 1a). Backscattering erases the conductance quantization. In two-dimensional geometries, in which conductance quantization has been studied extensively, scattering centers outside of the 1D constriction are less harmful to conductance quantization, as they will only affect the trajectories of a small percentage of electrons. Also, in a plane scattering less likely results in backscattering (Figure 1b). So far indications of conductance quantization in nanowires have been reported in Si/Ge core−shell nanowires,[24,25] while signs of quasi-ballistic transport, but no unambiguous conductance quantization, have been observed in InAs nanowires.[23,26−30]

Here we demonstrate quantization of conductance in InSb nanowires at nonzero magnetic field. We study the quantization as a function of source-drain bias and magnetic field. With this subband spectroscopy we extract the main characteristics of the system, namely, the Landé g factor and the subband spacing.

Received: September 21, 2012
Revised: December 13, 2012

dx.doi.org/10.1021/nl3035256 | *Nano Lett.* XXXX, XXX, XXX−XXX

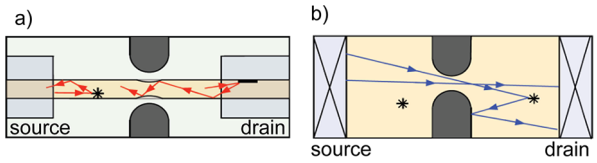

Figure 1. Consequences of scattering in nanowires and two-dimensional geometries. (a) Transport through a constriction in a nanowire. Scattering at an impurity reflects an electron back to the source reservoir. Reflection at the reservoirs, here drawn for the drain reservoir, also leads to backscattering. (b) Transport through a constriction in a two-dimensional geometry in the presence of scattering centers. Note that, compared to the 1D nanowire in panel a), a scatterer only affects a small number of the ballistic trajectories from source to drain reservoir and that scattering is less likely to lead to scattering through the 1D constriction.

Our device (Figure 2a) is an InSb nanowire with two metal contacts (Ti/Au). The InSb nanowires have a zinc blende crystal structure free of structural defaults[31] and have yielded field-effect mobilities up to 35 000 $cm^2\ V^{-1}\ s^{-1}$. The spacing of the two metal contacts in the device studied here (~200 nm) is comparable to the electron mean free path of ~300 nm extracted from measurements of field-effect mobility. Conductance quantization has however also been observed in a device with ~850 nm contact spacing A global backgate controls the electron density in the nanowire (Figure 2b). Differential conductance $g = dI/dV$ is measured using a standard lock-in technique. On application of an in-plane magnetic field conductance steps as a function of backgate voltage are observed as seen in Figure 2c. The conductance at the two plateaus is, after subtraction of 6 kΩ of series resistance, $g \approx 0.5g_Q$ and $g \approx 1g_Q$, corresponding to transport through the lowest subband 1↑ and through the 1↑ and 1↓ subband, respectively (see Figure 2d). Subbands are denoted by an index, with 1 the subband lowest in energy, and spin-split subbands (↑ or ↓) that are degenerate in the absence of magnetic field have the same number.

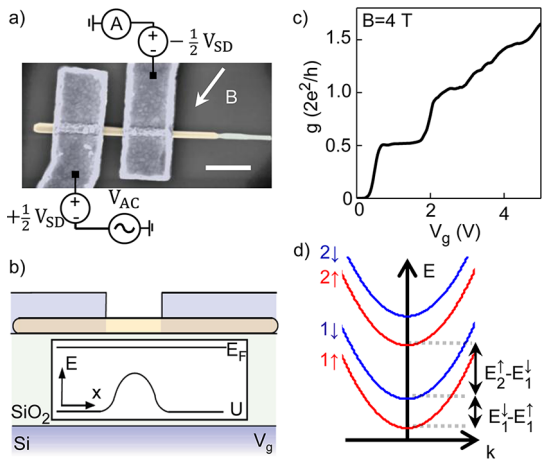

Figure 2. Quantization of conductance in an InSb nanowire. (a) Scanning electron microscope image of a contacted (Ti/Au 25/150 nm) InSb nanowire similar to the one measured. The InSb wire is colored yellow, the stem (InP and InAs) green. The direction of the in-plane magnetic field B with respect to the wire is indicated. The angle between nanowire and magnetic field is (53 ± 5)°. Differential conductance $g = dI/dV = I_{AC}/V_{AC}$ is obtained from a 50 μV_{RMS} excitation V_{AC}. The source-drain bias V_{SD} is applied antisymmetrically across the sample. The scale bar is 500 nm. All measurements were performed at a temperature of 4.2 K. (b) Schematic drawing of the nanowire lying on a Si substrate covered with 285 nm SiO_2. The highly p-doped Si acts as a global backgate to which a voltage V_g is applied. The inset shows the electrostatic potential U created by the backgate voltage V_g. The electrostatic potential leads to the formation of a constriction in the wire in the region between the two contacts. (c) Conductance g as a function of backgate voltage V_g at $B = 4$ T ($V_{SD} = 0$ mV) shows plateaus at 0.5 and 1.0 conductance quanta g_Q ($2e^2/h$). A series resistance of 6 kΩ has been subtracted, chosen such that the conductance of the second plateau is $1.0g_Q$. This series resistance, consisting of the impedance of the current amplifier (3 kΩ) and a contact resistance at the interface of the InSb wire and the metal contact, is discussed in more detail in the Supporting Information. (d) At nonzero magnetic field the energy spectrum consists of spin-split subbands $n\{\uparrow,\downarrow\}$. The energy spacing between subbands 1↓ and 1↑, where $g = 0.5g_Q$, is denoted as $E_1^\downarrow - E_1^\uparrow$. The energy spacing between 2↑ and 1↓ ($g = 1.0g_Q$) is denoted as $E_2^\uparrow - E_1^\downarrow$.

1D conductance channels show nonlinear conductance as a function of DC source-drain bias V_{SD}. So-called half-plateaus at intermediate conductance values $g \approx 0.25g_Q$, $0.75g_Q$, and larger fractions arise at high V_{SD} when the number of subbands available for electrons from source or drain reservoir differs by 1.[32−34] Nanowire conductance as a function of V_{SD} and gate voltage (Figure 3a) shows that the $0.5g_Q$ and $1.0g_Q$ plateaus around $V_{SD} = 0$ mV evolve into these intermediate plateaus at high source-drain bias ($V_{SD} \sim \pm 10$ mV). $g(V_g)$ traces at $V_{SD} =$ 0 mV, −7.5 mV, and −11 mV show the appearance of the high-bias plateaus (Figure 3b). The observation of these half-plateaus at high source-drain bias is a further confirmation of conductance quantization.

The derivative of conductance to gate voltage,[35] the transconductance dg/dV_g, of the same nonlinear transport data (Figure 3c) shows the subband alignment with respect to source and drain reservoir as a function of gate voltage and source-drain bias. Zero-bias and high-bias plateaus (zero transconductance) are separated by lines of high transconductance that arise when a subband aligns with source or drain reservoir. Two high transconductance lines intersect at finite V_{SD} when source and drain are aligned with successive subbands. This is seen in Figure 3c for the 1↑ and 1↓ subbands at $V_{SD} = 14$ mV (point marked with *). In this configuration[33] the source-drain potential eV_{SD} equals the subband spacing $E_1^\downarrow - E_1^\uparrow$, as depicted schematically in Figure 3d. We therefore extract an energy spacing $E_1^\downarrow - E_1^\uparrow(B = 4\ T)$, which is also the Zeeman energy at $B = 4$ T, of 14 meV.

Gate traces as a function of magnetic field B (Figure 4a) show that the conductance plateaus become more pronounced with increasing B. At $B = 0$ T conductance is dominated by resonances that obscure the plateaus. The resonances, which are discussed in the Supporting Information, are suppressed at higher magnetic fields, enabling observation of the $0.5g_Q$ plateau for $B \geq 2$ T and the $1.0g_Q$ plateau for $B \geq 3$ T. The improvement of plateau quality with magnetic field suggests the presence of orbital effects; similar to two-dimensional electron gases[36] application of a magnetic field seems to reduce backscattering.

The subband spacing $E_1^\downarrow - E_1^\uparrow$, obtained from voltage bias spectroscopy measurements such as the one shown in Figure 3c, increases with magnetic field as seen in Figure 4b. We extract from a linear fit with intercept fixed to zero to this Zeeman splitting a |g| factor of the first subband $|g_1| = 1/\mu_B\ d(E_1^\downarrow - E_1^\uparrow)/dB$ of 58 ± 1 (μ_B is the Bohr magneton). As the subband splitting at zero magnetic field is experimentally not accessible, also a linear fit with the intercept as a fitting

dx.doi.org/10.1021/nl3035256 | Nano Lett. XXXX, XXX, XXX−XXX

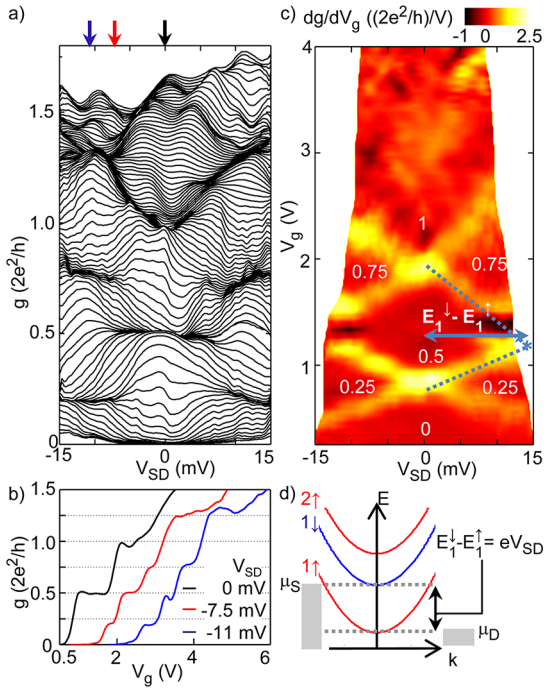

Figure 3. Voltage bias spectroscopy. (a) Conductance as a function of source−drain voltage V_{SD}. Each trace is taken with fixed V_g between −0.25 and 4 V and plotted without offset between traces. Dense regions correspond to conductance plateaus. Data obtained at B = 4 T. (b) Gate traces at V_{SD} = 0 mV (black), V_{SD} = −7.5 mV (red), and V_{SD} = −11 mV (blue), corresponding to the location of the arrows in panel a). The bump at $g = 0.5g_Q$ in the trace taken at V_{SD} = −11 mV is an electronics artifact. (c) Transconductance dg/dV_g of the data in panel a shows plateaus (zero transconductance, red) separated by transitions between plateaus with high transconductance (yellow/white). The conductance of the plateaus is indicated. The intersection of two regions of high transconductance surrounding the 0.5 plateau at finite V_{SD} (indicated with *) allows extraction of the energy $E_1^{\downarrow} - E_1^{\uparrow}$. (d) The intersection of the high-transconductance regions at high source-drain bias (point * in panel c) corresponds to the alignment of the electrochemical potential of the source with spin-split subband 1↓, while the drain potential is aligned with spin-split subband 1↑. The source−drain potential eV_{SD} equals the subband spacing $E_1^{\downarrow} - E_1^{\uparrow}$.

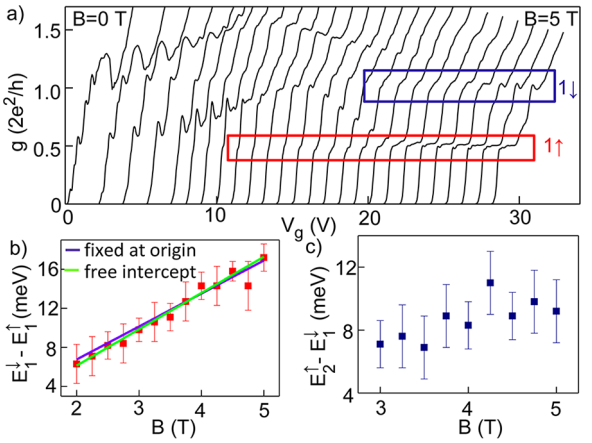

Figure 4. Development of the conductance plateaus in magnetic field. (a) Conductance g as a function of gate voltage V_g at B between 0 and 5 T in steps of 0.2 T. The $0.5g_Q$ and $1.0g_Q$ conductance plateaus are indicated by the red and blue box, respectively. (b) For B between 2 and 5 T the spin-split subband spacing $E_1^{\downarrow} - E_1^{\uparrow}$ is extracted from voltage bias spectroscopy measurements as indicated in panel 3c). From a linear fit through the origin (purple line) an effective $|g|$ factor $|g_1| = 58 \pm 1$ is obtained. A linear fit with the intercept as a free parameter (green line) gives $|g_1| = 64 \pm 3$. c) Spin-split subband spacing $E_2^{\uparrow} - E_1^{\downarrow}$ extracted from conductance as a function of source-drain bias and gate voltage (conductance plots in voltage bias spectroscopy measurements) between 3 and 5 T.

parameter is performed, giving a $|g_1|$ of 64 ± 3 . These g factors are higher than the bulk InSb $|g|$ factor of 51. Although spin−orbit interaction is thought to affect $|g|$ factors in confined geometries[37,38] our enhanced $|g|$ factor can likely be attributed to exchange enhancement in low density quantum point contacts.[39−41] A gradual increase of conductance with source-drain bias prevents observation of the transition between the $1.0g_Q$ plateau and the $1.25g_Q$ high-bias plateau in transconductance. The subband spacing between 2↑ and 1↓, $E_2^{\uparrow} - E_1^{\downarrow}$, is therefore extracted from measurements of conductance as function of source-drain bias and gate voltage (see Supporting Information), giving $E_2^{\uparrow} - E_1^{\downarrow}$ (3 T ≤ B ≤ 5 T) ∼ 10 meV (Figure 4c). The less well-defined $1.0g_Q$ plateau in voltage bias spectroscopy measurements complicates extraction of a clear magnetic field dependence of subband spacing $E_2^{\uparrow} - E_1^{\downarrow}(B)$.

In a second device conductance plateaus at $g = 0.5g_Q$ and $g = 1.0g_Q$ are observed as the out-of-plane magnetic field increases, showing the reproducibility of our results (Figure 5a). The $0.5g_Q$ plateau widens with field for $B \leq 5$ T, and from voltage bias spectroscopy measurements we extract $|g_1|$=51 ± 1 for a linear fit with intercept fixed to zero (the intercept as fitting parameter gives 62 ± 3) (Figure 5b). The $g = 0.5g_Q$ plateau remains approximately constant in width for $B > 5$ T. The $g = 1.0g_Q$ plateau is observed for $B \geq 5.75$ T, and its subband spacing, also obtained from voltage bias spectroscopy measurements, increases linearly with B for magnetic fields up to 9 T.

A transconductance plot of the gate traces of Figure 5a, in which the lines of high transconductance correspond to the onset of transport through a subband, shows that a crossing of two subbands occurs at $B \approx 5$ T (Figure 5c). We now explain which subbands cross and under which conditions a subband crossing occurs. At zero magnetic field the ↑ and ↓ subbands with the same index are degenerate, and Zeeman energy lifts the degeneracy at nonzero magnetic fields. This is seen in Figure 5c for the 1↓ and the 1↑ subband. One of the subbands involved in the crossing is therefore the 1↓ subband, and the similarity in slope to the 1↑ level at $B > 5$ T suggests that the second subband involved is the 2↑ subband. At nonzero B quantized steps with height $g = 1g_Q$ split into steps of height $g = 0.5g_Q$ (see first column of Figure 5d, where only the $0.5g_Q$ plateau is seen). When B is increased such that the Zeeman energy is equal to the energy spacing of subbands at B = 0 T, two subbands with opposite spin and an index that differs by 1 become degenerate. Two $0.5g_Q$ steps combine to a single $1.0g_Q$ step, leading to the disappearance of the plateaus at integer g_Q. As in our data at $B \sim 5$ T the 2↑ and 1↓ subband are degenerate, a $1.0g_Q$ step from $0.5g_Q$ to $1.5g_Q$ occurs (see second column of Figure 5d). At Zeeman fields larger than the subband spacing the order of subbands is changed, in our case to 1↑, 2↑, 1↓, and the width of the $0.5g_Q$ plateau, now defined as $E_2^{\uparrow} - E_1^{\uparrow}$, is, excluding magnetic field contributions to confinement, constant in magnetic field. The $1.0g_Q$ plateau grows as a larger magnetic field increases the Zeeman energy separation between 1↓ and 2↑. Both the constant width of the $0.5g_Q$ plateau as well

dx.doi.org/10.1021/nl3035256 | Nano Lett. XXXX, XXX, XXX−XXX

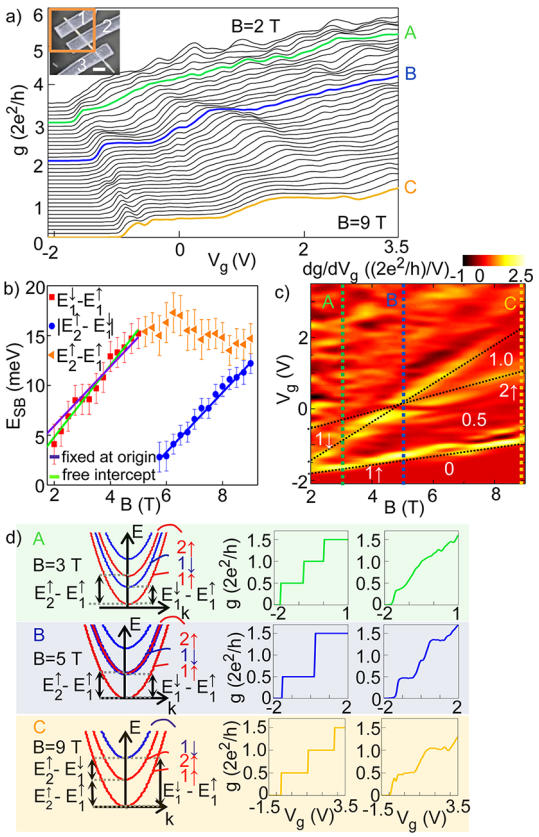

Figure 5. Conductance quantization and subband crossing in device II. (a) Conductance g as a function of V_g at out-of-plane B between 2 and 9 T in steps of 0.2 T. The green, blue and yellow trace (B = 3 T, 5 T, and 9 T, respectively) are shown in the right column of panel d). Inset: scanning electron microscopy image of device II with relevant contacts (1 and 2) and wire region indicated by the box. Contact spacing is 300 nm, wire diameter 70 nm. Scale bar is 500 nm. (b) Subband spacing E_{SB} as a function of B for spin-split levels $E_1^{\downarrow} - E_1^{\uparrow}$ ($g = 0.5g_Q$, red squares) and $|E_2^{\uparrow} - E_1^{\downarrow}|$ ($g = 1.0\ g_Q$, blue dots) obtained from voltage bias spectroscopy measurements. The purple and green lines are linear fits to $E_1^{\downarrow} - E_1^{\uparrow}$ with fit fixed at the origin and the intercept as a free parameter, providing $|g_1|$ = 51 ± 1 and 62 ± 3, respectively. The linear fit (blue line) to $|E_2^{\uparrow} - E_1^{\downarrow}(B)|$ gives $|g_{2-1}| = 1/\mu_B\, d(E_2^{\uparrow} - E_1^{\downarrow})/dB$ = 52 ± 2. The subband spacing of the $0.5g_Q$ plateau for B > 5 T is denoted by $E_2^{\uparrow} - E_1^{\uparrow}$ (orange triangles). (c) The transconductance dg/dV_g of the traces of panel a) shows the onset of transport through a subband as a line of high transconductance (yellow/white). Plateau conductance (zero transconductance; red) is indicated. With increasing B the spin-split subbands 1↓ and 1↑ move apart. Around B = 5 T 1↓ intersects with the 2↑ subband. Cuts A, B, and C are the magnetic field values (B = 3 T, 5 T, and 9 T, respectively) at which $g(V_g)$ is shown in panel d). Black dotted lines are a guide to the eye. (d) Schematic drawing of the subband energies at B = 3, B = 5, and B = 9 T (left) and the corresponding schematic conductance steps (middle). The right column shows measured gate traces at the indicated magnetic field.

as the increase in subband spacing of the $1.0g_Q$ plateau are seen in Figure 5a, b and c.

Crossings of spin-split subbands have been observed in quantum point contacts in GaAs two-dimensional hole and electron gases.[42,43] The large g factor in InSb, leading to a large Zeeman energy, makes such a subband crossing reachable at moderate magnetic fields. The energy spectrum of the wire between contacts 2 and 3 in the inset of Figure 5a shows similar signs of a subband crossing (see Supporting Information). In both wire sections it was found that a magnetic field affects the relative energy of subbands via a Zeeman energy contribution; a magnetic field contribution to confinement strength[44,45] was not observed.

The spin-degenerate subband spacing at B = 0 T is estimated from the subband crossing point. In the absence of magnetic field contributions to confinement strength $E_2^{\uparrow} - E_1^{\uparrow}$ equals the spin-degenerate subband spacing between the first two subbands; $E_2^{\uparrow} - E_1^{\uparrow} = E_2 - E_1$. At the degeneracy between the 2↑ and 1↓ subbands at $B \approx 5$ T $E_2^{\uparrow} - E_1^{\uparrow} = E_1^{\downarrow} - E_1^{\uparrow} \approx 15$ meV. We therefore estimate a spin-degenerate subband spacing $E_2 - E_1 \approx 15$ meV. This subband spacing agrees well with the level spacing $E_2 - E_1$ = 18 meV in an infinite cyclindrical well with diameter equal to our wire diameter (70 nm), which is, considering that the confinement potential in our nanowire is likely different from cylindrical, taken only as a rough estimate.

To summarize we have observed quantized conductance in InSb nanowires at nonzero magnetic fields. Subband spectroscopy, performed by measuring conductance quantization as a function of source−drain voltage and magnetic field, allowed extraction of Landé g factors of ∼55 and a subband spacing of ∼15 meV. Results reported here on devices with small contact spacing indicate quasi-ballistic rather than diffusive transport conditions in the InSb nanowire devices with contact spacing ∼1 μm used in detection of MFs. Moreover, observation of conductance plateaus is a prerequisite for detection of a helical liquid in a nanowire. Our results are therefore an essential step toward creation of such a helical state. The extracted nanowire characteristics also allow estimation of the experimental conditions under which a helical state arises. It is required[46] that spin−orbit energy E_{SO} and Zeeman energy are similar in size and therefore, based on the reported |g| factor and $E_{SO} \sim 50\ \mu$eV,[12] a magnetic field of ∼15 mT is predicted to lead to a helical state. Furthermore, subband spacings reported here are expected to be large enough to allow detection of helical liquid signatures on conductance plateaus. Future experiments will focus on nanowire devices with local gating, giving more control over the shape and location of confinement potential, to achieve ballistic transport at zero magnetic field, and will explore ballistic transport in nanowires in the presence of spin−orbit interaction.

■ ASSOCIATED CONTENT

Supporting Information

Fabrication details and electronic characterization of device I and II, an estimation of contact resistance, voltage bias spectroscopy measurements at 0 T of device I, measurements of conductance as function of source−drain bias and gate voltage of device I at 4 T, voltage bias spectroscopy measurements at 3 T, 5 T, and 9 T of device II, and a transconductance measurement of the energy spectrum in device II as function of magnetic field and gate voltage. This material is available free of charge via the Internet at http://pubs.acs.org.

■ AUTHOR INFORMATION

Corresponding Author

*E-mail: l.p.kouwenhoven@tudelft.nl.

Present Address

[§]Department of Physics and Astronomy, University of Pittsburgh, Pittsburgh, Pennsylvania 15260, United States.

Notes

The authors declare no competing financial interest.

■ ACKNOWLEDGMENTS

We thank M. van der Krogt for technical assistance. This work has been supported by The Netherlands Organization for Scientific Research (NWO), the Foundation for Fundamental Research on Matter (FOM) and Microsoft Corporation Station Q.

■ REFERENCES

(1) Lutchyn, R. M.; Sau, J. D.; Das Sarma, S. *Phys. Rev. Lett.* **2010**, *105*, 077001.
(2) Oreg, Y.; Refael, G.; Von Oppen, F. *Phys. Rev. Lett.* **2010**, *105*, 177002.
(3) Mao, L.; Gong, M.; Dumitrescu, E.; Tewari, S.; Zhang, C. *Phys. Rev. Lett.* **2012**, *108*, 177001.
(4) Kitaev, A. Y. *Phys. Usp.* **2001**, *44*, 131.
(5) Alicea, J.; Oreg, Y.; Refael, G.; von Oppen, F.; Fisher, M. P. A. *Nat. Phys.* **2011**, *7*, 412−417.
(6) Středa, P.; Šeba, P. *Phys. Rev. Lett.* **2003**, *90*, 256601.
(7) Kloeffel, C.; Trif, M.; Loss, D. *Phys. Rev. B* **2011**, *84*, 195314.
(8) Quay, C. H. L.; Hughes, T. L.; Sulpizio, J. A.; Pfeiffer, K. W.; Baldwin, K. W.; West, K. W.; Goldhaber-Gordon, D.; De Picciotto, R. *Nat. Phys.* **2010**, *6*, 336−339.
(9) Datta, S.; Das, B. *Appl. Phys. Lett.* **1990**, *56*, 665.
(10) Bratkovsky, A. M. *Rep. Prog. Phys.* **2008**, *71*, 026502.
(11) Žutić, I.; Fabian, J.; Das Sarma, S. *Rev. Mod. Phys.* **2004**, *76*, 323−410.
(12) Nadj-Perge, S.; Pribiag, V. S.; Van den Berg, J. W. G.; Zuo, K.; Plissard, S. R.; Bakkers, E. P. A. M.; Frolov, S. M.; Kouwenhoven, L. P. *Phys. Rev. Lett.* **2012**, *108*, 166801.
(13) Nilsson, H. A.; Samuelsson, P.; Caroff, P.; Xu, H. Q. *Nano Lett.* **2012**, *12* (1), 228−233.
(14) Mourik, V.; Zuo, K.; Frolov, S. M.; Plissard, S. R.; Bakkers, E. P. A. M.; Kouwenhoven, L. P. *Science* **2012**, *336*, 1003.
(15) Potter, A. C.; Lee, P. A. *Phys. Rev. Lett.* **2010**, *105*, 227003.
(16) Lutchyn, R. M.; Stanescu, T. D.; Das Sarma, S. *Phys. Rev. Lett.* **2011**, *106*, 127001.
(17) Stanescu, T. D.; Lutchyn, R. M.; Das Sarma, S. *Phys. Rev. B* **2011**, *84*, 144522.
(18) Potter, A. C.; Lee, P. A. *Phys. Rev. B* **2011**, *83*, 184520.
(19) Brouwer, P. W.; Dückheim, M.; Romito, A.; Von Oppen, F. *Phys. Rev. B* **2011**, *84*, 144526.
(20) Van Wees, B. J.; Van Houten, H.; Beenakker, C. W. J.; Williamson, J. G.; Kouwenhoven, L. P.; Van der Marel, D.; Foxon, C. T.; Harris, J. J. *Phys. Rev. Lett.* **1988**, *60*, 848.
(21) Wharam, D. A.; Thornton, T. J.; Newbury, R.; Pepper, M.; Ahmed, H.; Frost, J. E. F.; Hasko, D. G.; Peacock, D. C.; Ritchie, D. A.; Jones, G. A. C. *J. Phys. C* **1988**, *21*, L209.
(22) Shtrikman, H.; Popovitz-Biro, R.; Kretinin, A.; Kacman, P. *IEEE J. Sel. Top. Quantum Electron.* **2011**, *17*, 4.
(23) Kretinin, A. V.; Popovitz-Biro, R.; Mahalu, D.; Shtrikman, H. *Nano Lett.* **2010**, *10* (9), 3439−45.
(24) Lu, W.; Xiang, J.; Timko, B. P.; Wu, Y.; Lieber, C. M. *Proc. Natl. Acad. Sci. U.S.A.* **2005**, *102* (29), 10046−10051.
(25) Xiang, J.; Vidan, A.; Tinkham, M.; Westervelt, R. M.; Lieber, C. M. *Nat. Nanotechnol.* **2006**, *1*, 208−213.
(26) Ford, A. C.; Kumar, S. B.; Kapadia, R.; Guo, J.; Javey, A. *Nano Lett.* **2012**, *12*, 1340−1343.
(27) Zhuo, X.; Dayeh, S. A.; Aplin, D.; Wang, D.; Yu, E. T. *Appl. Phys. Lett.* **2006**, *89*, 053113.
(28) Doh, Y. J.; Roest, A. L.; Bakkers, E. P. A. M.; De Franceschi, S.; Kouwenhoven, L. P. *J. Korean Phys. Soc.* **2009**, *54*, 135.
(29) Thelander, C.; Björk, M. T.; Larsson, M. W.; Hansen, A. C.; Wallenberg, L. R.; Samuelson, L. *Solid State Commun.* **2004**, *05*, 0333.
(30) Hansen, A. E.; Björk, M. T.; Fasth, C.; Thelander, C.; Samuelson, L. *Phys. Rev. B* **2005**, *71*, 205328.
(31) Plissard, S. R.; Slapak, D. R.; Verheijen, M. A.; Hocevar, M.; Immink, G. G. W.; Van Weperen, I.; Nadj-Perge, S.; Frolov, S. M.; Kouwenhoven, L. P.; Bakkers, E. P. A. M. *Nano Lett.* **2012**, *12* (4), 1794−1798.
(32) Kouwenhoven, L. P.; Van Wees, B. J.; Harmans, C. J. P. M.; Williamson, J. G.; Van Houten, H.; Beenakker, C. W. J.; Foxon, C. T.; Harris, J. J. *Phys. Rev. B* **1989**, *39*, 8040.
(33) Patel, N. K.; Nicholls, J. T.; Martin-Moreno, L.; Pepper, M.; Frost, J. E. F.; Ritchie, D. A.; Jones, G. A. C. *Phys. Rev. B* **1991**, *44*, 10973.
(34) Glazman, L. I.; Khaetskii, A. V. *JETP Lett.* **1988**, *48*, 591−595.
(35) The transconductance dg/dV_g is therefore a double derivative $dg/dV_g = d/(dV_g)(dI/dV)$ to current I.
(36) Van Wees, B. J.; Kouwenhoven, L. P.; Willems, E. M. M.; Harmans, C. J. P. M.; Mooij, J. E.; van Houten, H.; Beenakker, C. W. J.; Williamson, J. G.; Foxon, C. T. *Phys. Rev. B* **1991**, *43*, 12431.
(37) Csonka, S.; Hoffstetter, L.; Freitag, F.; Oberholzer, S.; Schönenberger, C.; Jespersen, T. S.; Aagesen, M.; Nygård, J. *Nano Lett.* **2008**, *8* (11), 3932−3935.
(38) Nilsson, H. A.; Caroff, P.; Thelander, C.; Larsson, M.; Wagner, J. B.; Wernersson, L.-A.; Samuelson, L.; Xu, H. Q. *Nano Lett.* **2009**, *9* (9), 3151−3156.
(39) Thomas, K. J.; Nicholls, J. T.; Simmons, M. Y.; Pepper, M.; Mace, D. R.; Ritchie, D. A. *Phys. Rev. Lett.* **1996**, *77*, 135.
(40) Cronenwett, S. M.; Lynch, H. J.; Goldhaber-Gordon, D.; Kouwenhoven, L. P.; Marcus, C. M.; Hirose, K.; Wingreen, N. S.; Umansky, V. *Phys. Rev. Lett.* **2002**, *88*, 22.
(41) Frolov, S. M.; Venkatesan, A.; Yu, W.; Folk, J. A. *Phys. Rev. Lett.* **2009**, *102*, 116802.
(42) Daneshvar, A. J.; Ford, C. J. B.; Hamilton, A. R.; Simmons, M. Y.; Pepper, M.; Ritchie, D. A. *Phys. Rev. B* **1997**, *55*, 20.
(43) Graham, A. C.; Thomas, K. J.; Pepper, M.; Cooper, N. R.; Simmons, M. Y.; Ritchie, D. A. *Phys. Rev. Lett.* **2003**, *91*, 13.
(44) Berggren, K.-F.; Thornton, T. J.; Newson, D. J.; Pepper, M. *Phys. Rev. Lett.* **1986**, *57*, 1769−1772.
(45) Wharam, D. A.; Ekenberg, U.; Pepper, M.; Hasko, D. G.; Ahmed, H.; Frost, J. E. F.; Ritchie, D. A.; Peacock, D. C.; Jones, G. A. C. *Phys. Rev. B* **1989**, *39*, 9.
(46) Pershin, Y. V.; Nesteroff, J. A.; Privman, V. *Phys. Rev. B* **2004**, *69*, 121306(R).